



Morphology of Atmospheric Particles over Semi-Arid Region (Jaipur, Rajasthan) of India: Implications for Optical Properties

Sumit Kumar Mishra^{1*}, Rajesh Agnihotri¹, Pawan Kumar Yadav¹, Sukhvir Singh¹, M.V.S.N. Prasad¹, Puppala Siva Praveen², Jai Shankar Tawale¹, Rashmi¹, Nidhi Dixit Mishra³, Bhuwan Chandra Arya¹, Chhemendra Sharma¹

¹ CSIR-National Physical Laboratory, New Delhi, 110012, India

² International Centre for Integrated Mountain Development, Kathmandu, GPO Box 3226, Nepal

³ Division of Environmental Sciences, Indian Agricultural Research Institute, New Delhi, 110012, India

ABSTRACT

The regional dust morphology and spectral refractive indices (RIs; governed by hematite, Fe₂O₃ content at short wavelengths) are key elements for ascertaining direct radiative forcing of mineral dust aerosols. To provide morphological features of background mineral dust from a semi-arid zone in the vicinity of the Thar Desert, we carried out an expedition to the Jaipur city during late winter of 2012. Morphological analysis reveals the predominance of “Layered”, “Angular” and “Flattened” particles, while the frequency distribution of a total of 235 dust particles shows the aspect ratio, AR and circularity parameter, CIR (measures of particle’s non-sphericity) typically ~1.4 and ~0.8, respectively. Sensitivity analysis at 550 nm wavelength reveals the equivalent sphere model may underestimate Single Scattering Albedo, SSA for the dust with low (~1.1%) hematite by ~3.5%. Both underestimation (by ~5.6%) and overestimation (up to 9.1%) are probable in case of dust with high hematite content (~5.68%). In addition, the effect of AR on the dust scattering is significant in case of dust with high hematite content. More such regionally representative dust morphological data are required for better estimation of regional radiative forcing of mineral dust aerosols.

Keywords: Dust; Morphology; Hematite; Refractive index; SSA.

INTRODUCTION

The direct radiative forcing (DRF) imposed by aerosol remains still uncertain to large extent (Boucher *et al.*, 2013). The effective radiative forcing due to aerosol–radiation interactions (ERF_{ari}) via mineral dust aerosols has been reported to be –0.1 (–0.3 to +0.1) Wm^{–2} (Boucher *et al.*, 2013). Generally, the mineral dust sources are associated with arid regions with low rainfall (annual rainfall < 200–250 mm). The arid zones are often affected/extended due to droughts, climate shifts and human activities like inappropriate agriculture practices, overgrazing and deforestation etc. (Prospero *et al.*, 2002). North Africa is the largest mineral dust source region in the world where Bodélé Depression (northern Chad) plays crucial role in dust emission (Engelstaedter *et al.*, 2006) by contributing up to 18% of global dust emissions (Todd *et al.*, 2007). Besides this, Middle

East, Central Asia and South Asia are the other persistent sources for the mineral dust (Prospero *et al.*, 2002). Mineral dust is radiatively very important in the atmosphere due to its widespread distribution and relatively high optical depth (Sokolik and Toon, 1996; Tegen *et al.*, 1997). The morphological (shape and size) analyses of atmospheric particles using Scanning Electron Microscopes (SEMs) reveal that the shapes of dust particles are extremely irregular (Buseck and Pósfai, 1999). The morphological factors such as shape, sharpness of edges and surface texture (i.e., the degree of surface roughness) affect the single scattering properties of a particle. The light scattering of a single particle is affected mostly by three key factors: the size of the scatterer compared to the wavelength, its shape, and its refractive index, *m* (*m* of atmospheric aerosols depends on their chemical composition). The aerosol optical properties; Single Scattering Albedo (SSA), Asymmetry Parameter (*g*) and Extinction Efficiency (*Q_{ext}*) are numerically estimated by utilizing region specific dust morphological and chemical composition information obtained from ground based and in-situ aircraft observations.

In general, for current modeling practices, radiative transfer simulations and remote sensing implementations, shape of

* Corresponding author.

Tel.: +91-11-4560-8621; Fax: +91-11-4560-2263

E-mail address: sumitkumarm@gmail.com

dust particles is assumed to be homogenous sphere so that the classical Lorenz-Mie theory can be used. However, based on the measurement and modeling studies (accounting for particle morphology), the optical properties of real dust particles have been found to be quite different compared to that of volume-equivalent spheres (Volten *et al.*, 2005; Mishra and Tripathi, 2008). Therefore, to improve our current understanding about radiative properties of mineral dust, the information on regional dust morphology is needed.

Microscopy-based techniques for individual particle characterization with a brief overview of major particle types, their identification, and their sources have been reviewed by Pósfai and Buseck (2010). They emphasized the importance of characterization of physical and chemical properties of individual aerosol particles that may contribute to climate effects. Imaging techniques have been used as the valuable tools for the categorization of the atmospheric particles throughout the world (Okada *et al.*, 2001; Okada and Kai, 2004; McDonald and Biswas, 2004). However, in whole Asia, most of the studies for dust characterization are limited to the Chinese Deserts.

In context to India, the Great Indian Desert (also known as the Thar Desert) is known as the local source of mineral dust in South Asia. Satellite observations, back trajectory analysis, and chemical analysis support the fact that the Thar Desert is the local source of mineral dust (Deepshikha *et al.*, 2005; Chinnam *et al.*, 2006; Moorthy *et al.*, 2007) which spreads over an area of 0.32×10^6 km² in the north-west part of India. To the best of our knowledge, there is no study from the Thar Desert which reports the detailed morphology of regional aerosols. Hence, a series of field observations are being carried out in the region to provide a statistically significant database which could be fed in the optical and radiative models to understand their impact on regional climate. This study is a part of aforesaid campaigns where regional atmospheric particles have been collected from Jaipur (a semi-arid zone, Rajasthan, in vicinity of the Thar Desert) during late winter, 2012 for studying the individual particle morphology and the chemical composition. The companion paper (Agnihotri *et al.*, 2015) from the Jaipur field experiment reports the mineralogical composition of particles at bulk and at individual particle level while this manuscript presents detailed morphology of background mineral dust, the standard nomenclature of particle shapes based on NIST (National Institute of Standards and Technology) library, inferences on individual particle composition based on SEM-EDS spot analysis, spectral variation of refractive indices of regional dust particles and finally the sensitivities of dust morphology and hematite content on the optical properties of dust at the visible wavelength (550 nm).

STUDY REGION

As a first step, the experiment was carried out in Jaipur (26.89°N, 75.81°E), a semi-arid zone close to the Thar Desert. It is the state capital of Rajasthan surrounded by various old forts situated on semi-arid mountains such as Nahargarh and Jaigarh with the altitude range 800–1000 m

from ground level. The aerosol sampling has been carried out on the aforementioned forts together with Kukas hill (at height ~800 m from ground in vicinity of industrial zone), Kukas NH8 (highway near Kukas hill), Makarana (~110 km west of Jaipur, representative of mining and grinding zone of marbles) and Birla temple (which lies within the city) during February, 2012. These sites are representative of their regional local topography/geology. Thus, overall sampling was carried out at six sites of Jaipur with varying altitude including one faraway site (i.e., Makarana) representing active mining area. Fig. 1 shows the geo-position of all of the sampling sites, few sites with their atmospheric backgrounds and the particle sampler. Sampling sites with their geographical positions, sampling dates with contemporary local meteorological parameters over the sites are given in Table 1.

THEORETICAL FRAMEWORK, EXPERIMENTAL DETAILS AND METHODOLOGY

Basic morphological parameters of aerosols are calculated based on earlier studies (Okada *et al.*, 2001; Kalashnikova and Sokolik, 2004):

- (1) Maximum projection (or the length of the longest projected dimension): the largest separation between points on the particle convex perimeter.
- (2) Width (w): the particle's largest length perpendicular to the maximum projection.

The aforesaid has been depicted in Fig. 3(a).

- (3) Area and Perimeter: projected area and perimeter of individual particles.

Maximum projection, width, area and perimeter of individual particles have been calculated using image J software (<http://rsbweb.nih.gov/ij/>).

Using these parameters, the basic morphological parameters are derived which are common in literature. These are aspect ratio (AR), circularity (CIR) and Volume Equivalent Radius (VER).

$$AR = \frac{\text{maximum projection}}{\text{width}} \quad (1)$$

Aspect ratio of a sphere is equal to one;

$$CIR = 4\pi \times \frac{\text{area}}{\text{perimeter}^2} \quad (2)$$

where, area and perimeter mean the area and perimeter of the individual particle targeted in the SEM image whose CIR is to be calculated. VER is the radius of a sphere of same volume as that of the non-spherical particle. The parameter VER of a non-spherical particle is calculated by equating its volume with that of same volume sphere.

$$\text{Volume of a non-spherical particle} = \text{particle area} \times \text{particle thickness} \quad (3)$$

$$\text{Volume of a sphere} = (4/3) \times \pi \times r^3 \quad (4)$$

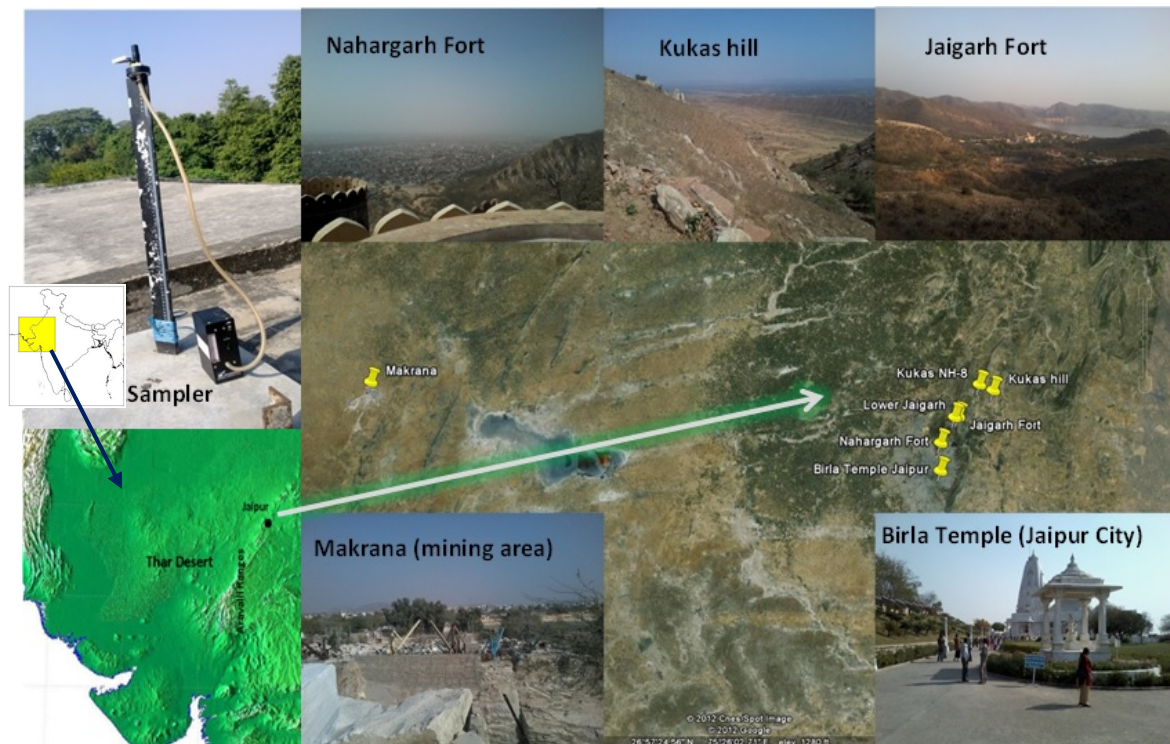


Fig. 1. Geographical location of the sampling sites, portable handheld PM_5 sampler and some of the sampling sites with their atmospheric backgrounds.

Table 1. Sampling sites with their geo-position, date of sample collection and some local meteorological parameters over the sampling sites. *Meters Above Ground Level (MAGL).

Sampling site	Date (Feb, 2012)	Latitude	Longitude	Approx. height of sampling site (*MAGL)	Weather	Wind direction	Avg. wind speed (km/h)
Jaigarh Fort	20	26.982	75.844	1000	Partly sunny	W-SW	7
Nahargarh Fort	21	26.94	75.816	800	Sunny day with mild dust storm	W	10–30
Kukas near NH-8	22	27.036	75.892	10	Clear sky	E	5
Kukas hill	22	27.027	75.919	800	Sunny	E	15–17
Makarana mining area	23	27.042	74.714	50	Mostly sunny	W	15–17
Birla Temple	25	26.893	75.816	10	Sunny	N	4

Due to limitations for the particle thickness observation in this paper, we utilized the thickness information for particles collected from Chinese arid regions (Okada *et al.*, 2001) which show that the thickness of individual particles is 0.3 times of particle width. Volume of a non-spherical particle has been calculated using aforesaid relationship, width and area of individual particles in Eq. (3). Now, the Volume Equivalent Radius ($r = VER$) has been estimated after comparing Eqs. (3) and (4).

In this paper, we calculated CIR following approach by Okada *et al.* (2001). The parameters AR and CIR, both give information on extent of particle non-sphericity. However, AR is generally used as the major input parameter for calculation of optical properties of non-spherical particles while CIR is used for generation of shape distribution.

Ambient atmospheric particles [PM_5 (particles with

aerodynamic diameter $< 5 \mu m$) and few TSP samples] were collected using a low volume air sampler (APM 801, Envirotech) with air flow rates generally kept as 1.5 L/min (LPM). The topological features, surface morphologies and individual particle elemental chemical composition were studied using a Scanning Electron Microscope (SEM: ZEISS EVO MA-10) equipped with an energy dispersive spectrometer (EDS: Oxford Link ISIS 300) facility. SEM is capable of resolving 3nm size particle at 30KV accelerating voltage. Energy dispersive spectrometer attached to the SEM can identify the elements having atomic nos. of the elements from beryllium (Be) to uranium (U) with an accuracy of 133 eV.

Based on the earlier studies, it has already been shown that the smaller particles (particle diameter $\leq 2.5 \mu m$) reside in the atmosphere for a prolonged time and hence more prone to interact with incoming solar radiation compared

to that of large particles (Seinfeld and Pandis, 1998). The presence of larger particles over the desert can't be ignored especially during summer time when strong convection gives rise in their number; however, the study (Miller *et al.*, 2006) reported that the contribution of bigger particles to the total global annual averaged dust load is negligible. Their modeling study revealed that the total global annual averaged dust load in the atmosphere is mainly due to dust particles of radii $< 10 \mu\text{m}$ where particles with radii $1\text{--}2 \mu\text{m}$ contribute to it the most. In present study, we collected $\text{PM}_{2.5}$ and TSP samples. TSP samples were collected for few sites only.

For investigating the bulk chemical composition of particles using XRF facility, $\text{PM}_{2.5}$ particles were collected on pre-weighed Teflon (diameter 37 mm) filters using $\text{PM}_{2.5}$ sampler. For individual particle morphology and chemical composition (using spot EDS) analysis, particles were collected on the Tin substrates ($\sim 1 \times 1 \text{ mm}^2$; thickness $\sim 0.1 \text{ mm}$). Before sampling, the marked (at a corner side) tin substrate was placed on the Teflon filter such that the marked facet should be the exposure side during particle collection. The exposed tin substrate was collected after 2 hour exposure and carefully stored in small micro-biological specimen tube labeled with sample specifications. These specimen tubes were then stored in the desiccator until the analysis. The scanning of the particles deposited on the tin substrate is done manually through the microscope during SEM analysis. The recorded SEM images reveal the shape and geometrical size of the individual particles. For calculation of surface area, perimeter and AR of individual particles observed in the SEM images, Image J software has been used. Thus estimated area and perimeter of individual particles have been used for the calculation of CIR (as discussed above).

Thus, in this study over all 235 dust particles were analyzed for estimation of morphological parameters. Carbonaceous particles (fractal like morphology; emitting due to vehicular, combustion activity etc.) and pollens were not considered for AR and CIR calculation as they are not dust particles and have been identified based on their characteristic morphology and spot EDS information (if available).

RESULTS AND DISCUSSIONS

Nomenclature of Shapes of the Atmospheric Particles Based on NIST Database

NIST recommended a practice guide (Jillavenkatesa *et al.*, 2001) which emphasizes the importance of standard nomenclature for particle shapes for the better measurements of their size distribution. This is very important for the atmospheric particles especially mineral dust which is highly non-spherical and predominant over the desert regions. The region-specific dust particle shape information may be helpful to reduce the uncertainty in particle size distribution by accounting for the shape factor of representative shapes over that region (DeCarlo *et al.*, 2004; Slowik *et al.*, 2004).

To define the particle shapes with standard nomenclature, we have used NIST morphology glossary (<http://www.nist.gov/lispix/doc/particle-form/part-morph-gloss.htm>).

The SEM images of selected sampled particles with their names as per NIST morphology glossary have been shown in Fig. 2. Most of the particles shown belong to $\text{PM}_{2.5}$ size. In addition, a few TSP (bulk size) particles are also shown.

As Fig. 2(A) (A-1–A-3) depicts, particles from Birla temple site named as quadrangular, rounded layered structure, grape like structure and aggregate. As this sampling site lies within the city so some signatures of pollution were traced by spot EDS analysis of individual particles. Grape like structure is nothing but the big aged carbon fractal comprising of carbon monomers. Due to combustion/vehicular emission activities, fresh carbon fractals (open long chain fractals) are released in the atmosphere which reside in the atmosphere for long time and form close fractals (closed chain compact fractal) due to surface tension and particle dynamics. EDS analysis of the particle reveals that the particle is rich in carbon and sulfur. The sulfur may be forming a layer on each monomer during aging process in the atmosphere. The rounded stratified layered particle was termed as rounded layered particle. The quadrangular particle is basically a deformed cubic particle rich in NaCl while the aggregate particle was found to be rich in CaCO_3 based on EDS data. The particle compositions were inferred based on spot EDS data.

The TSP particles over Kukas NH8 [Fig. 2(B) (B-1)] were found with thick, rough, broken or discontinuous layer on the surface and are termed as crust particles. At this site, we also found some rounded shaped particles with specific shape pattern. These particles may be pollens. As these particles were also found over other sampling site (Kukas hill) so these may belong to Kukas area.

Over Jaigarh site [Fig. 2(C) (C-1–C-3)], we found some very flat two dimensional triangular structures (termed as triangular flake structure), particles with parallel layers on the surface (termed as layered structures) and flattened rounded crust like structured particles. The flattened structures are of oblate shape and thicker than the flakes. Based on EDS analysis, layered structure particles were inferred to be rich in calcite and quartz. Again, over Kukas NH8 [Fig. 2(D) (D-1)], we found flattened shaped particles.

Over Nahargarh fort [Fig. 2(E) (E-1–E-3)], in general we found sharp edged particles termed as angular particles. Angular crust like particle was found to be rich in quartz while some angular particles were found to be rich in C, N, O and Si. The later may be originally quartz particle where aging would have occurred. The curved or crooked particles with relatively rounded grooves are termed as bent structures with channels.

Over Makarana sampling site [Fig. 2(F) (F-1)] which is representative of grinding and mining area of marbles, particles were found to be smooth, angular with conchoidal fractures. These particles were termed as glass like angular particles.

The TSP particles sampled over Kukas hill [Fig. 2(G) (G-1–G-4)], shows the majority of rounded shape particles with a unique pattern (may be pollen) which we have discussed earlier. We have also captured some particles which seem to be of biogenic origin with deformed hollow

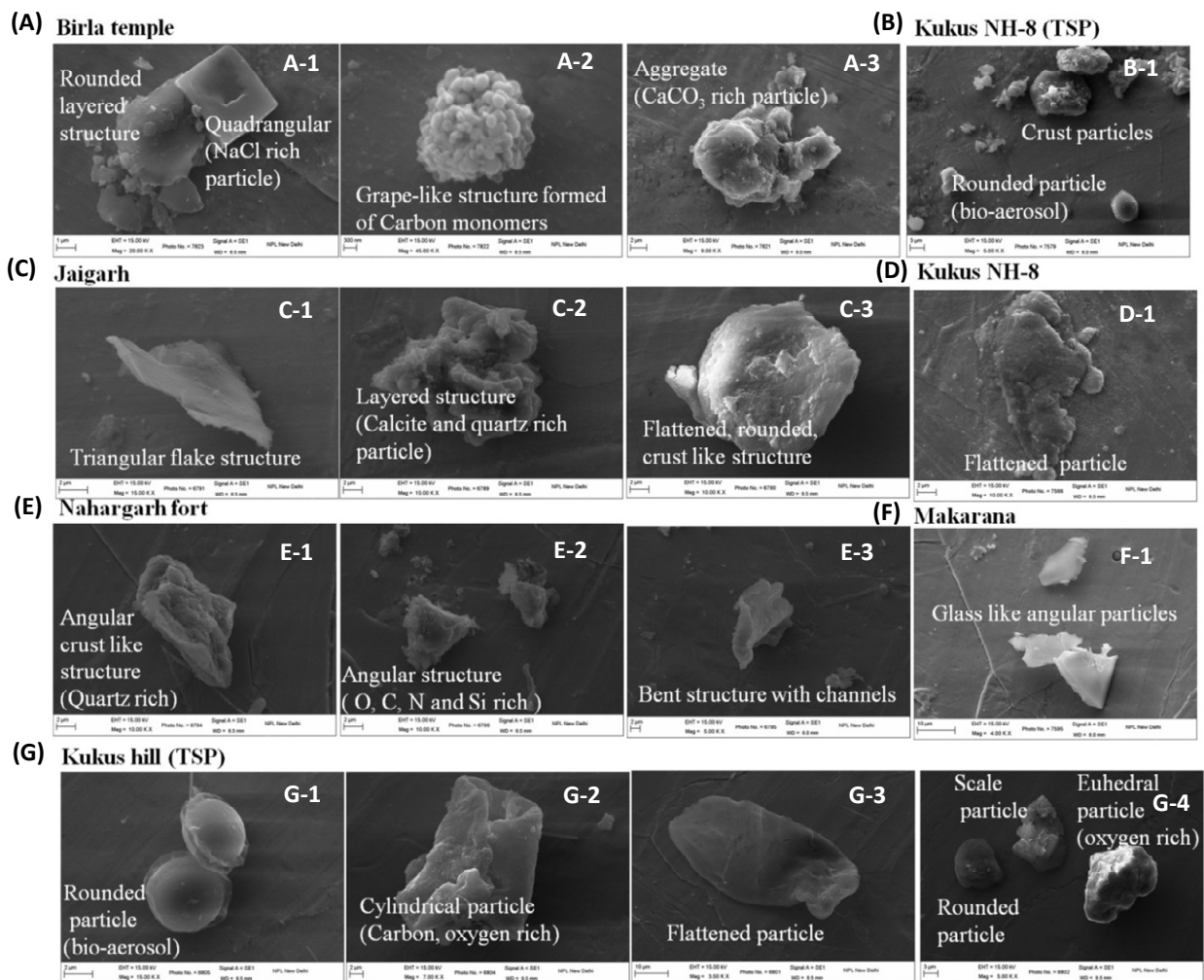


Fig. 2. Particle morphology based on NIST database together with individual particle composition for selected particles.

cylindrical (rich in C and O) and flattened shape. At the same site, we observed the particles with thin broken or discontinuous layer on surface (termed as scale particle), particles with nearly all flat surfaces (termed as euhedral particle) and the rounded particles. The euhedral particle was found to be rich in O.

“Layered”, “Angular” and “Flattened” dust particles were found to be dominant over all the sites. Here, anthropogenic (which were limited to Birla temple site) and biogenic particles were filtered out based on their characteristic morphology and not counted as dust particles. The information on particle shape is valuable to modelers for deciding/designing the model shapes for the optical/radiative simulation of dust particles over the study region. But only this shape information is not sufficient. For the simulation of dust optical properties, one requires the information on the morphological parameters which have been discussed in the following sections.

Morphological Parameters (AR, CIR) of Sampled Dust

Fig. 3(c1) and 3(c2) show the frequency distribution of AR and CIR for the total dust particles sampled from the sites considered in this study (except the Lower Jaigarh

Fort where the tin substrate could not be collected due to some technical problem). Based on AR and CIR distributions shown in Figs. 3(c1) and 3(c2), particles with AR = 1.4 and CIR tending to 0.8 were found to be dominant. The kernel fits over the AR and CIR distributions for particles with VER < 2 μm, > 2 μm and all VER reveal the same fact. Here, it is noteworthy that the AR and CIR for spherical particles are 1 (AR = CIR = 1). Higher AR values and lower CIR values represent particle non-sphericity. Fig. 3(c3) shows the number distribution of the dust particles with VER together with kernel fit over the distribution. Micron radius particles were found to be predominant over all the sites. Among all the sampling sites, the highest AR was found to be 5.4 for the particles sampled over Makarana mining area which may give rise to highly non-spherical particles in the atmosphere due to local grinding and mining activities. The average AR and CIR (with their respective standard deviation) of PM₅ particles for all the sites have been given in Table 2. The particles over Kukus hill show lowest AR (1.52) while the particles over Makarana show highest AR (1.76). The AR and CIR for the whole study region has been found to be 1.64 ± 0.64 and 0.73 ± 0.14, respectively.

Kandler *et al.* (2007) reported the AR to be 1.64 for the

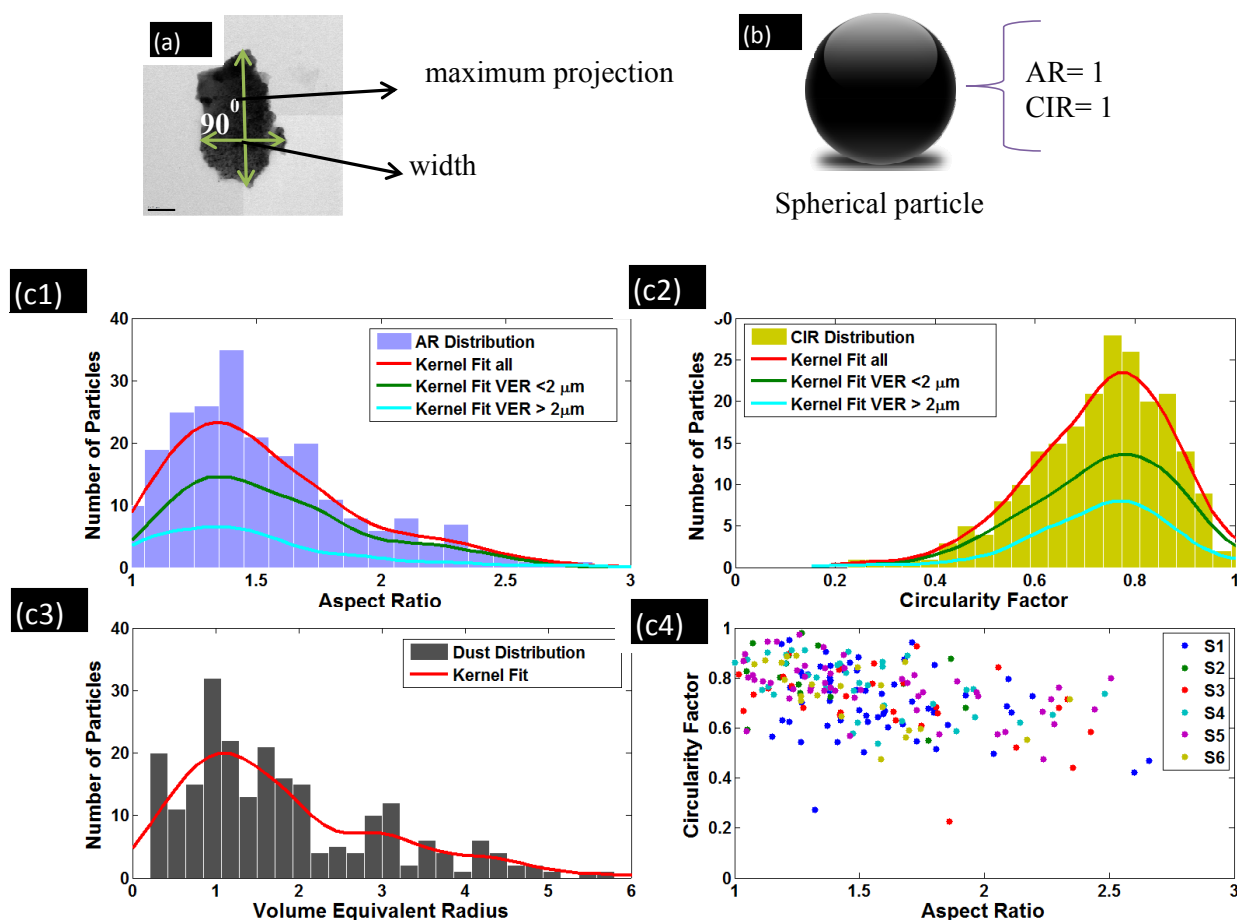


Fig. 3. (a) Maximum projection of a particle together with particle width (b) volume equivalent sphere of the non-spherical particle shown in (a). (c1) frequency distribution of Aspect Ratio, AR for all the analyzed particles (c2) same as c1 but for Circularity Factor, CIR (c3) size distribution of all the analyzed particles (c4) correlation of AR and CIR for all the particles sampled from the sites s1 to s6. The AR and CIR for the spherical particle is one.

Table 2. Average AR and CIR for the sampling sites.

Site	AR	CIR
Jaigarh	1.61 ± 0.40	0.71 ± 0.14
Nahargarh	1.75 ± 1.02	0.72 ± 0.20
Kukas NH8	1.60 ± 0.57	0.71 ± 0.16
Kukas hill	1.52 ± 0.35	0.77 ± 0.11
Makarana	1.76 ± 0.89	0.75 ± 0.13
Birla Temple	1.56 ± 0.49	0.73 ± 0.13

Saharan Mineral Dust collected at Izana, Tenerife (Spain), while higher value of AR to be 1.9 have been reported (Reid *et al.*, 2003) for African mineral dust collected over the Caribbean after being transported over the North Atlantic Ocean. Median AR of 1.6 has been reported (Kandler *et al.*, 2009) for the dust particles (size > 0.5 μm) collected over west Saharan Desert. Another study (Coz *et al.*, 2009) reported a median average value of AR to be 1.81 based on the individual particle characterization from North Africa. Study conducted over the Chinese Deserts reported the median AR to be 1.4 for mineral particles with radius 0.1–6 μm (Okada *et al.*, 2001). The dust morphological study during Asian dust storms (from China) by Parungo (1997)

revealed the AR to be 1.5.

In a very simplistic approach, based on frequency distributions of AR and CIR over the semi-arid zone under this study (Fig. 3), one can simulate the optical properties of PM₅ mineral dust by considering the dust particles with AR to be 1.4 and CIR to be 0.8. However, in place of considering single dust model shape corresponding to a single CIR value, it is always better to consider the dust shape distribution (CIR with VER) together with particle size distribution for accurate numerical estimation of dust optical properties (Kalashnikova and Sokolik, 2004; Kalashnikova *et al.*, 2005).

Spectral Variation of Refractive Indices of Mineral Dust

In general, the error arising due to spherical model approximation is assumed to be negligible compared to the errors associated with other sources, however, the case studies (Kahnert *et al.*, 2005; and the references therein) showed that the net-flux error caused by the use of spherical model particles are comparable to the error caused by the uncertainty in the refractive index. Hence, together with particle morphology, the information on spectral variation of refractive indices of mineral dust is also very important for their optical/radiative simulation.

The companion paper (Agnihotri *et al.*, 2015) reports the chemical composition of mineral dust with a range of hematite weight percentage [key component for governing refractive indices at shorter wavelengths (Mishra and Tripathi, 2008; Mishra *et al.*, 2008; Mishra *et al.*, 2012)] in mineral dust over the semi-arid zone. Agnihotri *et al.* (2015) calculated hematite weight percentage from elemental oxide data where they assumed that all Fe is present as hematite of density 5.3 gm/cc. Now, using the density of mineral dust (2.65 gm/cc), the volume fractions of hematite has been computed. Following the approach (Mishra and Tripathi, 2008), spectral refractive index (real and imaginary) of mineral dust has been calculated using Bruggman's effective medium mixing rule (Bohren and Huffman, 1998; 217 pp.) at wavelengths 550, 670, 860, and 1020 nm. The volume percentage of hematite [with the minimum and maximum occurrence, 1.10–5.68 over the arid zone; expect Kukas Hill where high Fe (hematite) contribution may be due to anthropogenic activity] (Agnihotri *et al.*, 2015) has been used as metallic percentage while the non-metallic proportion has been constrained based on measurements (Peterson, 1968) for simulation of refractive indices. Fig. 4(a) shows the variation of real part of refractive index with the considered wavelengths for the minimum and maximum percentage of hematite while Fig. 4(b) shows the same but for imaginary part of refractive indices.

Values of n and k were found to increase with increasing hematite fraction. Between the two hematite percentages, the deviation in “ n ” is significant at 550 nm wavelength and the same is true for “ k ”. In case of Fig. 4(b), the deviations diminish with increasing wavelengths. Both the indices (n and k) fall with increasing wavelengths for the considered hematite percentages. Similar spectral variation of “ k ” was reported for the Saharan dust (Carlson and Caverly, 1977). The refractive indices of the dust particles [clay component with varying hematite volume percentage] (Lafon *et al.*,

2006) support the overall trend of spectral variation of indices in this study. The increase in hematite content (from 1.10 to 5.68%) was found to enhance the “ k ” to 5.6-fold at 550 nm wavelength. Using Spectral Optical Absorption Photometer (SOAP) and the retrieval technique, the spectral variation of imaginary part of the complex refractive index, k , for the five Saharan dust samples (i.e., Cairo 2, Burkina Faso, SAMUM B1, SAMUM B2, SAMUM B3) have been estimated (Wagner *et al.*, 2012). Modeled spectral variation of “ k ” for the mineral dust over the study site exhibits similar spectral variation as that of Saharan dust samples. “ k ” for Saharan dust samples have been shown with uncertainties for comparison with that of Indian desert dust.

Sensitivity of Dust Morphology and Mineralogy to Mineral Dust Optics

As it is well known that the visible radiation of the incoming solar radiation interacts most of the aerosol species existing in the earth's atmosphere. Hence, for studying the sensitivity of dust morphology and mineralogy (especially hematite content) to the mineral dust optics, optical properties of dust particles have been computed for some model shapes (refer Fig. 5(a); model shapes are with AR 1.5 and 1.6 and VER to be 1.2 μm) at wavelength 550 nm.

The optical properties (such as SSA and extinction efficiency) of the mineral dust with VER 1.2 μm , have been computed using Discrete Dipole Approximation, DDA model (Draine and Flatau, 2004; <http://arxiv.org/abs/astro-ph/0409262v2>). Major inputs to the DDA code are: refractive index, wavelength (μm), VER of the non-spherical particle, particle shape and the particle shape parameters. AR of the particle and its spread in the X, Y and Z directions, is governed by the shape parameters. The outputs of the code are extinction, scattering and absorption efficiencies (Q_{ext} , Q_{sca} and Q_{abs}), g , and the scattering matrix elements. The

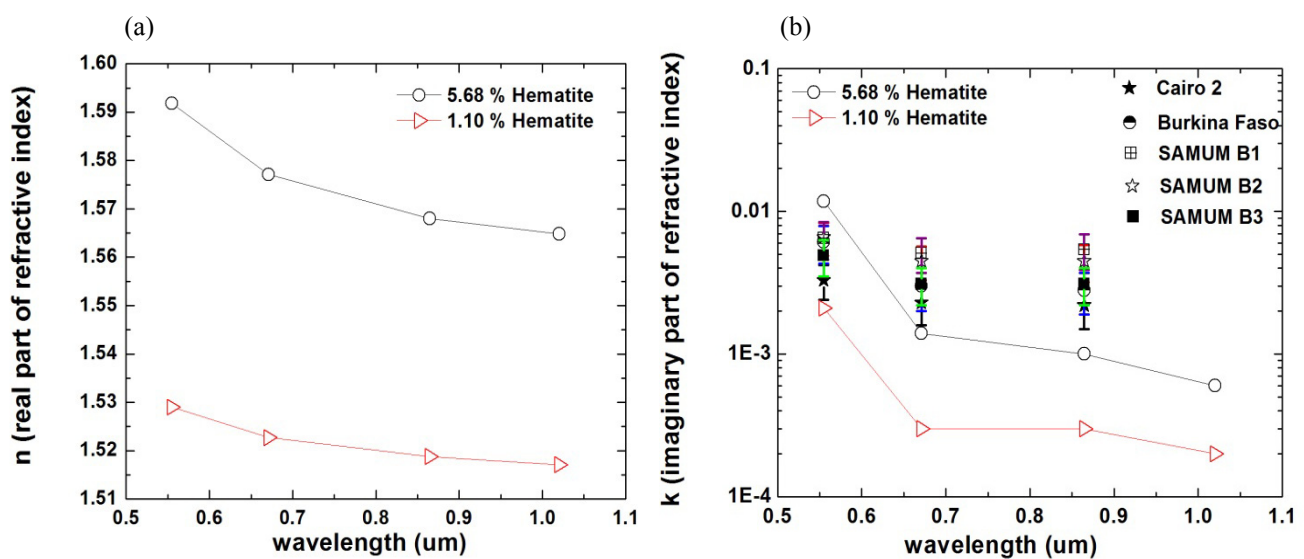


Fig. 4. Spectral variation of refractive indices (a) real part, n and (b) imaginary part, k for the 1.10 and 5.68 % (volume) hematite content in mineral dust. The spectral variation of “ k ” for five Saharan dust samples (i.e., Cairo 2, Burkina Faso, SAMUM B1, SAMUM B2, SAMUM B3) have also been shown with associated uncertainties from a recent study (Wagner *et al.*, 2012).

DDA code has been tested and verified with the earlier published results (Kalashnikova and Sokolik, 2004; Mishra et al., 2012) for exactly similar conditions.

During SSA calculation with the DDA model, dust particles with varying shapes but same size (representative VER 1.2 μm from Fig. 3(c3)) have been considered. Here, the refractive indices of mineral dust at 550 nm wavelength corresponding to the minimum (1.10%) and the maximum (5.68%) amount of hematite content (Fig. 4) have been used for the simulation of dust optical properties.

Fig. 5(a) shows, the observed dust morphologies and their model shapes together with the volume equivalent sphere. For understanding the effect of dust morphology on its optics, model shapes have been considered based on the particle morphology observed in this study over the arid region. Based on the observations, following particles have been considered as Model shapes:

1) Rectangular Grain (RG): based on the appearance of the particle (resembles a rectangular bar), a rectangular solid of length, l has been considered. For simplicity, width (w) and height (thickness; h) have been assumed to be same i.e., $w = h$.

2) Rectangular Plate (RP): the rectangular flat plate has been considered as model shape to represent the particle which seems to have very small thickness. Here, the thickness (h) has been considered as “ $h = 0.3 w$ ” where w is width of the particle.

3) Hexagon Plate (HXP): a hexagon flat plate has been

considered as model shape to represent the hexagon shape flat particle. Here, thickness of the particle has been assumed in the same way as has been considered for Rectangular Plate (RP). For simplicity, all the sides of hexagon model shape have been considered of equal length.

4) Ellipsoid (ELP): to represent the oblate shaped particle with less thickness, an ellipsoidal particle (axis $a \neq b \neq c$) with semi-major axis, “ a ” and semi-minor axis “ b ” and “ c ” has been considered. Here, thickness ($2c$) of the particle has been incorporated as “ $c = 0.3 b$ ”.

5) Spheroid (SPD): for representing the thick oblate shaped particle, a spheroidal particle (axis $a \neq b = c$) has been considered as model shape. Here, thickness ($2c$) of the particle has been incorporated as $c = b$.

6) Triangular Plate (TRP): the triangular prism (sides a , b and c) with small thickness has been considered as model shape for the observed triangular flake particle. Here, for simplicity, two arms ($a = b$) of the triangular facets have been considered of same length but smaller than the third side (c). The thickness of the model shape has been considered as in case of RP, HXP and ELP.

Fig. 5(b) shows the SSA for the entire model shapes (with AR values 1.5 and 1.6 and VER 1.2 μm) and the refractive indices (from Fig. 4) at 550 nm wavelength. The SSA corresponding to high (5.68 %) and low hematite (1.10 %) have been found to be 0.768 and 0.936, respectively for the volume equivalent spheres with radius 1.2 μm ; the same has been shown with the dashed horizontal lines in the figure.

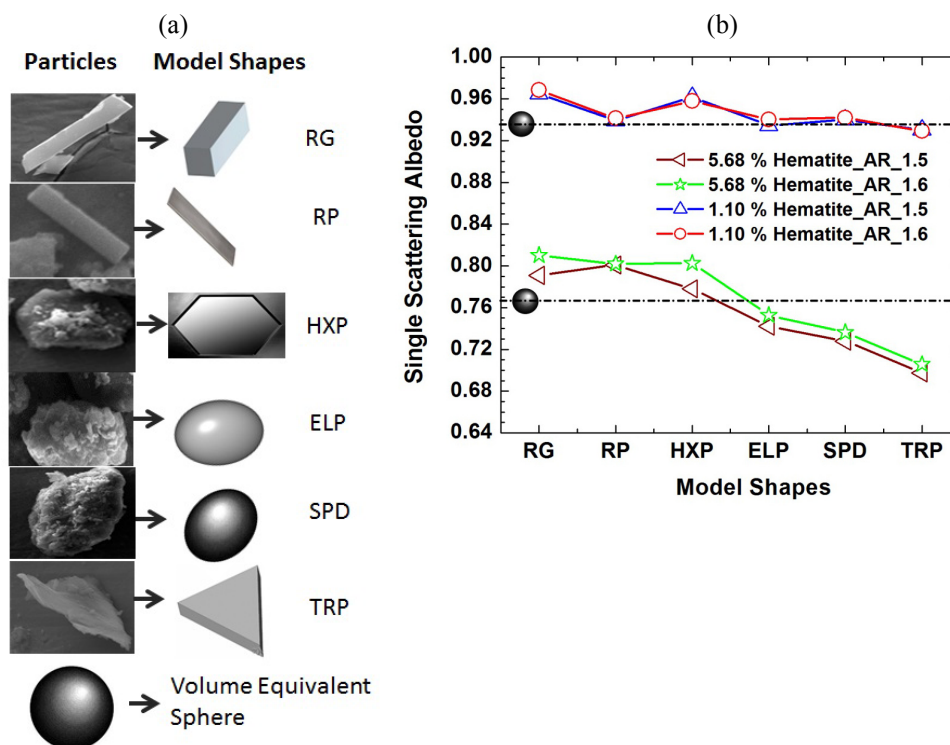


Fig. 5. (a) Images of individual particles and their equivalent model shapes (Rectangular Grain, RG; Rectangular Plate, RP; Hexagon Plate, HXP; Ellipsoid, ELP; Spheroid, SPD; and Triangular Plate, TRP) together with their volume equivalent sphere (b) numerically estimated Single Scattering Albedo, SSA (at 550 nm wavelength) for the model shapes (shown in (a)) with AR values 1.5 and 1.6 for given VER 1.2 μm and minimum (1.10%) and maximum (5.68%) hematite content in mineral dust.

In case of mineral dust with low hematite content (1.10%), all the model shapes except TRP, scatter more (or nearly same) compared to that of their volume equivalent sphere. Model RG shows the highest deviation followed by HXP from their equivalent sphere for both the aspect ratios (3.5% followed by 2.3% for AR 1.6; and 3.1% followed by 2.8% for AR 1.5). In case of low hematite, the effect of AR on the dust optics is not significant.

In case of mineral dust with high hematite content (5.68%), some model shapes (RG, RP and HXP) scatter more while other (ELP, SPD and TRP) scatter less compared to that of their volume equivalent sphere. Model shape TRP shows the highest deviation amongst all the model shapes from their equivalent sphere for both the aspect ratios (8.1% for AR 1.6 and 9.1% for AR 1.5). Compared to low hematite, the effect of AR on the dust optics is significant in case of high hematite content. In general, the scattering was found to increase with increase in AR of model shapes.

The effect of particle non-sphericity on mineral dust optics is significant in case of mineral dust with high hematite content. Hence, the non-sphericity of the dust particles must not be ignored in case of dust rich in hematite. In low hematite dust, SSA may be underestimated by considering equivalent sphere model while for high hematite dust, there is huge uncertainty involved in SSA (it may be underestimated or over estimated by considering equivalent sphere model) that depends on the proportions of particle shapes which govern SSA. So, a statistical representative database of regional dust morphology is needed, which may help to reduce the SSA uncertainty significantly. The observed dust morphology and spectral refractive indices (governed by hematite content) will refine the earlier radiative forcing estimation (Mishra *et al.*, 2008).

To access the change in radiative properties from that of routine based spherical particle assumption, the radiative forcing estimations have been carried out for one nonspherical particle case [i.e., the triangular plate (TRP; Fig. 5) with aspect ratio 1.5 and high hematite content 5.68% (by volume)] and its equivalent sphere with similar composition. As we know that the aerosol radiative forcing is a function of the aerosol optical properties [SSA; g (asymmetry parameter) and Q_{ext} (Extinction efficiency)] so we fed these simulated optical properties as input in the Santa Barbara Discrete Ordinate Radiative Transfer (SBDART) model (Ricchiuzzi *et al.*, 1998) to study the forcing variation from that of equivalent sphere. The forcing simulations reveal that the TRP shape shows higher cooling at surface (4.3%) and TOA (10.3%) while more atmospheric heating (3.2%) relative to that of their equivalent sphere.

CONCLUSIONS

A field observation has been conducted over a semi-arid zone in the vicinity of the Thar Desert during late winter of 2012 to carry out morphological analysis of regional aerosols. Morphological analysis reveals the predominance of “Layered”, “Angular” and “Flattened” particles whereas the frequency distribution of a total of 235 dust particles showed the aspect ratio, AR and circularity parameter, CIR

typically ~ 1.4 and ~ 0.8 , respectively. Based on numerical estimation of optical properties at 550 nm wavelength using DDA optical model, we found that the equivalent sphere model may underestimate SSA for the dust with low ($\sim 1.1\%$) hematite by $\sim 3.5\%$. Both underestimation (by $\sim 5.6\%$) and overestimation (up to 9.1%) are probable in case of dust with high hematite content ($\sim 5.68\%$). However, the occurrence of underestimation or overestimation relative to equivalent sphere model can be well determined by generating statistical representative database on proportions of particle shapes over the region. The effect of particle nonsphericity (evaluated in term of AR) on the dust scattering is significant in case of dust with high hematite content. Hence, morphological characterization of dust particles is a must for hematite rich dust. The observed dust morphology and modeled spectral refractive indices will refine the earlier radiative forcing estimation.

ACKNOWLEDGEMENTS

The authors are thankful to Director NPL, Prof. R. C. Budhani for his consistent support for the ongoing work. Authors also acknowledge CSIR Network Project AIM_IGPHim (PSC-0112) for the financial support. S K Mishra is thankful to Indo-US Science and Technology Forum for the financial support for presenting this work in AGU fall meeting, 2012; Dr Shankar G. Aggarwal for the rigorous review of the paper.

SUPPLEMENTARY MATERIALS

Supplementary data associated with this article can be found in the online version at <http://www.aaqr.org>.

REFERENCES

- Agnihotri, R., Mishra, S.K., Yadav, P., Singh, S., Rashmi, Prasad, M.V.S.N., Arya, B.C. and Sharma, C. (2015). Bulk Level to Individual Particle Level Chemical Composition of Atmospheric Dust Aerosols (PM_{2.5}) over a Semi-arid Zone of Western India (Rajasthan). *Aerosol Air Qual. Res.* 15: 58–71.
- Bohren, C.F. and Huffman, D.R. (1998). *Absorption and Scattering of Light by Small Particles*. John Wiley Inc., New York.
- Boucher, O., Randall, D., Artaxo, P., Bretherton, C., Feingold, G., Forster, P., Kerminen, V.M., Kondo, Y., Liao, H., Lohmann, U., Rasch, P., Satheesh, S. K., Sherwood, S., Stevens, B. and Zhang, X.Y. (2013). Clouds and Aerosols. In *Climate Change 2013: The Physical Science Basis. Contribution of Working Group I to the Fifth Assessment Report of the Intergovernmental Panel on Climate Change*, Stocker, T.F., Qin, D., Plattner, G.K., Tignor, M., Allen, S.K., Boschung, J., Nauels, A., Xia, Y., Bex, V. and Midgley, P.M. (Eds.), Cambridge University Press, Cambridge, United Kingdom and New York, NY, USA.
- Buseck, P.R. and Pósfai, M. (1999). Airborne Minerals and Related Aerosol Particles: Effects on Climate and the Environment. *Proc. Nat. Acad. Sci. U.S.A.* 96: 3372–

- 3379.
- Carlson, T.N. and Caverly, R.S. (1977). Radiative Characteristics of Saharan Dust at Solar Wavelengths. *J. Geophys. Res.* 82: 3141–3152.
- Chinnam, N., Dey, S., Tripathi, S.N. and Sharma, M. (2006). Dust Events in Kanpur, Northern India: Chemical Evidence for Source and Implications to Radiative Forcing. *Geophys. Res. Lett.* 33: L08803.
- Coz, E., Gómez-Moreno, F.J., Pujadas, M., Casuccio, G.S., Lersch, T.L. and Artiñano, B. (2009). Individual Particle Characteristics of North African Dust under Different Long-range Transport Scenarios. *Atmos. Environ.* 43: 1850–1863.
- DeCarlo, P., Worsnop, D.R., Slowik, J.G., Davidovits, P. and Jimenez, J.L. (2004). Particle Morphology and Density Characterization by Combined Mobility and Aerodynamic Diameter Measurements. Part 1: Theory. *Aerosol Sci. Technol.* 38: 1185–1205.
- Deepshikha, S., Satheesh, S.K. and Srinivasan, J. (2005). Regional Distribution of Absorbing Efficiency of Dust Aerosols over India and Adjacent continents Inferred Using Satellite Remote Sensing. *Geophys. Res. Lett.* 32: L08811.
- Draine, B.T. and Flatau, P.J. (2004). User Guide for the Discrete Dipole Approximation Code DDSCAT 6.1.
- Engelstaedter, S., Tegen, I. and Washington, R. (2006). North African Dust Emissions and Transport. *Earth Sci. Rev.* 79: 73–100.
- Jillavenkatesa, A., Dapkunas, S.J. and Lum, L.S. H. (2001). Particle Size Characterization (NIST Recommended Practice Guide), Materials Science and Engineering Laboratory, Special Publication 960-1, National Institute of Standards and Technology, Spec. Publ.
- Kahnert, M., Nousiainen, T. and Veihelmann, B. (2005). Spherical and Spheroidal Model Particles as an Error Source in Aerosol Climate Forcing and Radiance Computations: A Case Study for Feldspar Aerosols. *J. Geophys. Res.* 110: D18S13.
- Kalashnikova, O.V. and Sokolik, I.N. (2004). Modeling the Radiative Properties of Non-spherical Soil-derived Mineral Aerosols. *J. Quant. Spectrosc. Radiat. Transfer* 87: 137–166.
- Kalashnikova, O.V., Kahn, R., Sokolik, I.N. and Li, W.H. (2005). Ability of Multiangle Remote Sensing Observations to Identify and Distinguish Mineral Dust Types: Optical Models and Retrievals of Optically Thick Plumes. *J. Geophys. Res.* 110: D18S14.
- Kandler, K., Benker, N., Bundke, U., Cuevas, E., Ebert, M., Knippertz, P., Rodríguez, S., Schütz, L. and Weinbruch, S. (2007). Chemical Composition and Complex Refractive Index of Saharan Mineral Dust at Izaña, Tenerife (Spain) Derived by Electron Microscopy. *Atmos. Environ.* 41: 8058–8074.
- Kandler, K., Schütz, L., Deutscher, C., Ebert, M., Hofmann, H., Jäckel, S., Jaenicke, R., Knippertz, P., Lieke, K., Massling, A., Petzold, A., Schladitz, A., Weinzierl, B., Wiedensohler, A., Zorn, S. and Weinbruch, S. (2009). Size Distribution, Mass Concentration, Chemical and Mineralogical Composition, and Derived Optical Parameters of the Boundary Layer Aerosol at Tinfou, Morocco, during SAMUM 2006. *Tellus Ser. B* 61: 32–50.
- Lafon, S., Sokolik, I.N., Rajot, J.L., Caquineau, S. and Gaudichet, A. (2006). Characterization of Iron Oxides in Mineral Dust Aerosols: Implications for Light Absorption. *J. Geophys. Res.* 111: D21207.
- McDonald, R. and Biswas, P. (2004). A Methodology to Establish the Morphology of Ambient Aerosols. *J. Air Waste Manage. Assoc.* 54: 1069–1078.
- Miller, R.L., Cakmur, R.V., Perlwitz, J., Geogdzhayev, I.V., Ginoux, P., Koch, D., Kohfeld, K.E., Prigent, C., Ruedy, R., Schmidt, G.A. and Tegen, I. (2006). Mineral Dust Aerosols in the NASA Goddard Institute for Space Sciences ModelE Atmospheric General Circulation Model. *J. Geophys. Res.* 111: D06208.
- Mishra, S.K. and Tripathi, S.N. (2008). Modeling Optical Properties of Mineral Dust over the Indian Desert. *J. Geophys. Res.* 113: D23201.
- Mishra, S.K., Dey, S. and Tripathi, S.N. (2008). Implications of Particle Composition and Shape to Dust Radiative Effect: A Case Study from the Great Indian Desert. *Geophys. Res. Lett.* 35: L23814.
- Mishra, S.K., Tripathi, S.N., Aggarwal, S.G. and Arola, A. (2012). Optical Properties of Accumulation Mode Polluted Mineral Dust: Effects of Particle Shape, Hematite Content and Semi-external Mixing with Carbonaceous Species. *Tellus Ser. B* 64: 18536, doi: 10.3402/tellusb.v64i0.18536.
- Moorthy, K.K., Babu, S.S., Satheesh, S.K., Srinivasan J. and Dutt, C.B.S. (2007). Dust Absorption over the “Great Indian Desert” Inferred Using Ground-based and Satellite Remote Sensing. *J. Geophys. Res.* 112: D09206.
- Okada, K., Heintzenberg, J., Kai, K. and Qin, Y. (2001). Shape of Atmospheric Mineral Particles Collected in three Chinese Arid-regions. *Geophys. Res. Lett.* 28: 3123–3126.
- Okada, K. and Kai, K. (2004). Atmospheric Mineral Particles Collected at Qira in the Taklamakan Desert, China. *Atmos. Environ.* 38: 6927–6935.
- Pósfai, M. and Buseck, P. (2010). Nature and Climate Effects of Individual Tropospheric Aerosol Particles. *Annu. Rev. Earth Planet. Sci.* 38: 17–43.
- Parungo, F. (1997). *Asian Dust Storms and Their Effect on Radiation and Climate: Part 4*, Science and Technological Report 3134 for NOAA.
- Peterson, J.T. (1968). *Measurements of Atmospheric Aerosols and Infrared Radiation over Northwest India and Their Relationships*, Ph.D. Thesis, Department of Meteorology, University of Wisconsin, Madison, Wisconsin, USA.
- Prospero, J.M., Ginoux, P., Torres, O., Nicholson, S.E. and Gill, T.E. (2002). Environmental Characterization of Global Sources of Atmospheric Soil Dust Derived from the NIMBUS7 TOMS Absorbing Aerosol Product. *Rev. Geophys.* 40: 2-1–2-31, doi: 10.1029/2000RG000095.
- Reid, E.A., Reid, J.S., Meier, M.M., Dunlap, M.R., Cliff, S.S., Broumas, A., Perry, K. and Maring, H. (2003). Characterization of African Dust Transported to Puerto Rico by Individual Particle and Size Segregated bulk Analysis. *J. Geophys. Res.* 108: 1–22, doi: 10.1029/2002

- JD002935.
- Ricchiuzzi, P., Yang, S., Gautier, and Sowle, D. (1998). SBDART: A Research and Teaching Software Tool for Plane-parallel Radiative Transfer in the Earth's Atmosphere. *Bull. Am. Meteorol. Soc.* 79: 2101–2114.
- Seinfeld, J.H. and Pandis, S.N. (1998). *Atmospheric Chemistry and Physics*, John Wiley and Sons Inc, New York.
- Slowik, J.G., Stainken, K., Davidovits, P., Williams, L.R., Jayne, J.T., Kolb, C.E., Worsnop, D.R., Rudich, Y., DeCarlo, P.F. and Jimenez, J.L. (2004). Particle Morphology and Density Characterization by Combined Mobility and Aerodynamic Diameter Measurements. Part 2: Application to Combustion-Generated Soot Aerosols as a Function of Fuel Equivalence Ratio. *Aerosol Sci. Technol.* 38: 1206–1222.
- Sokolik, I.N. and Toon, O.B. (1996). Direct Radiative Forcing by Anthropogenic Airborne Mineral Aerosols. *Nature* 381: 681–683.
- Tegen, I., Hollrig, P., Chin, M., Fung, I., Jacob, D. and Penner, J. (1997). Contribution of Different Aerosol Species to the Global Aerosol Extinction Optical Thickness: Estimates from model Results. *J. Geophys. Res.* 102: 23895–23915.
- Todd, M.C., Washington, R., Martins, J.V., Dubovik, O., Lizcano, G., M'Bainayel, S. and Engelstaedter, S. (2007). Mineral Dust Emission from the Bodélé Depression, Northern Chad, during BoDEX 2005. *J. Geophys. Res.* 112: D06207.
- Volten, H., Muñoz, O., Hovenier, J.W., Haan, J.F., de Vassen, W., van der Zande, W.J. and Waters, L.B.F.M. (2005). WWW Scattering Matrix Database for Small Mineral Particles at 441.6 and 632.8 nm. *J. Quant. Spectrosc. Radiat. Transfer* 90: 191–206.
- Wagner, R., Ajtai, T., Kandler, K., Lieke, K., Linke, C., Müller, T., Schnaiter, M. and Vragel, M. (2012). Complex Refractive Indices of Saharan Dust Samples at visible and near UV Wavelengths: A Laboratory Study. *Atmos. Chem. Phys.* 12: 2491–2512, doi: 10.5194/acp-12-2491-2012.

Received for review, October 9, 2014

Revised, January 2, 2015

Accepted, January 14, 2015

Supplementary Materials

Technical Details for SEM-EDS analysis:

The exposed tin substrate was mounted on conducting carbon tape with side contacts of silver paste. These specimens were also coated (very fine coating) with Gold-Palladium target to enhance electrical conductivity of the samples for better contrast and imaging. Finally, the specimen is ready for surface morphological analysis using SEM. Marked facet is exposed to electron gun to analyze the shape and size of the individual particles under scan. The scanning of the particles deposited on the tin substrate is done manually through the microscope. The micrographs were recorded at different magnification across the specimen with resolution of 3nm in secondary mode at 30KV accelerating voltage. SEM micrographs reveal the shape and size of the individual particles as well as group of particles scattered on tin substrate. Elemental analysis of observed particles with different shape and size were carried out using EDS attached to SEM facility. The Si-Li detector was used in EDS analysis having resolution of 133eV with detection limit of 1 % (quantitative) and 0.5 % (qualitative).

Model details:

DDA method computes light scattering for randomly oriented spherical and non-spherical particles such as spheres, ellipsoids, rectangular, triangular and hexagonal solid shapes etc. DDA works well within the size parameter, $\alpha < 15$.

Graphic for manuscript:

